ChemPlusChem

Research Article
doi.org/10.1002/cplu.202400613

Chemistry Europe
European Chemical Societies Publishing

www.chempluschem.org

Phenoxazinone Synthase-Like Catalytic Activity of Bi- and Trinuclear Copper(II) Complexes with 2-Benzylethanolamine: Experimental and Theoretical Investigations

Oksana V. Nesterova,[a] Olena E. Bondarenko,[b] Armando J. L. Pombeiro,[b] and Dmytro S. Nesterov*[a]

The self-assembly reaction of 2-benzylaminoethanol (Hbae) with $CuCl_2$ or $Cu(NO_3)_2$ leads to the formation of binuclear $[Cu_2(bae)_2(Cl)_2]$ (**1**) and $[Cu_2(Hbae)_2(bae)_2](NO_3)_2$ (**2**) complexes, while the trinuclear $[Cu_3(Hbae)_2(bae)_2(dmba)_2](NO_3)_2$ (**3**) compound was obtained using the auxiliar bulky substituted 2,2-dimethylbutyric acid (Hdmba). Crystallographic studies reveal the molecular structures of **1** and **2** based on the similar $\{Cu_2(\mu\text{-}O)_2\}$ core, while the structure of **3** features the $\{Cu_3(\mu\text{-}O)_2\}$ core with consecutive arranement of the metal centres, supported by the additional carboxylate bridges. The strong intermolecular hydrogen bonds join the molecular structures into 1D (for **1** and **3**) or 2D (for **2**) architectures. All three compounds act as catalysts for the aerobic oxidation of 2-aminophenol to the phenoxazinone chromophore (phenoxazinone synthase-like activity) with the maximum reaction rates up to 2.3×10^{-8} M s^{-1}. The substrate scope involves methyl-, nitro- and chloro-substituted 2-aminophenols, disclosing the negligible activity of nitro-derivatives, while the 6-amino-*m*-cresol substrate shows the highest activity with the initial reaction rate of 5.8×10^{-8} M s^{-1}. The mechanism of the rate-limiting reaction step (copper-catalysed formation of 2-aminophenoxyl radicals) was investigated at the DFT level. The combined DFT and CASSCF studies of the copper superoxo Cu^{II}-OO· radical species as possible unconventional reaction intermediates resulted in a rational mechanism of H-atom abstraction, where the activation energies follow the experimental reactivity of substituted 2-aminophenols. The TDDFT and STEOM-DLPNO-CCSD theoretical calculations of the absorption spectra of substrates, phenoxazinone chromophores and putative polynuclear species containing 2-aminophenoxo ligand are reported.

Introduction

Phenoxazinone synthase (PHS) is a multicopper metalloenzyme, which catalyses the oxidative coupling of two 2-aminophenol derivatives to phenoxazinone chromophore during the biosynthesis of actinomycin D, a naturally occurring antitumor agent, as well as of phenoxazinone-based antibiotics.[1] PHS can be isolated in a low-activity dimeric and a high-activity hexameric oligomeric forms which are distinct molecular structures and cannot be transformed from each other by a simple association-dissociation equilibrium. Since the isolation[2] of PHS in 1962 and solving its crystal structure[3] in 2006 a lot of studies devoted to the creation of a bioinspired models bearing structural and functional properties of PHS have been performed.[4] Considering that the active site of PHS comprises several copper centres,[3] the primary focus in synthesizing artificial complexes for PHS-like activity was addressed to coordination compounds of copper of various nuclearities.[5] The compounds of other 3d metals were also studied, among them those of Zn,[6] Ni,[7] Co,[8] Mn,[9] as well as heterometallic Cu/M[10] ones. In many cases it was observed that polynuclear coordination compounds reveal a higher activity than that observed for mononuclear ones, clearly indicating the advantage of closely located catalytically active metal centres. These observations are in line with an effect of enhanced activity of polynuclear coordination compounds recognized in many areas of catalysis.[11]

The commonly studied model reaction for PHS-like activity is the aerobic coupling of 2-aminophenol into the phenoxazinone chromophore in the presence of a catalyst.[4a] However, despite numerous reports, many details of the respective reaction mechanisms remain unknown. This is the consequence of the fact that in most of the cases the 2-aminophenol coupling studies are done under similar conditions, being typically limited to the investigation of rate dependences on the substrate concentration only. The catalytic coupling of substituted 2-aminophenol substrates is rarely investigated,[1c,12] while the reports of theoretical studies of reaction mechanisms of this catalytic reaction are single.[12b,13] This contrasts to the strong interest of synthetic organic chemistry and O_2 activation topics in the metal-free and meta-catalysed aerobic oxidations of (amino)phenols.[14]

[a] *O. V. Nesterova, D. S. Nesterov*
Centro de Estudos de Engenharia Química, Instituto Superior de Engenharia de Lisboa, Instituto Politécnico de Lisboa, R. Conselheiro Emídio Navarro 1, 1959-007 Lisboa, Portugal
E-mail: dmytro.nesterov@vis.isel.pt

[b] *O. E. Bondarenko, A. J. L. Pombeiro*
Centro de Química Estrutural, Institute of Molecular Sciences, Departamento de Engenharia Química, Instituto Superior Técnico, Universidade de Lisboa, Av. Rovisco Pais 1, 1049-001 Lisboa, Portugal

Supporting information for this article is available on the WWW under https://doi.org/10.1002/cplu.202400613

Flexible aliphatic and Schiff base N,O-donor ligands are among the most commonly applied classes of ligands used to construct metal complex catalysts for PHS-like activity.[4a,15] The polydentate nature of these ligands as well as their variety of coordination modes facilitate the formation of close-packed molecules of different nuclearities and topologies, and, at the same time, allow partial decoordination and formation of unsaturated environments around the metal centres. Recently we reported the mono- and tetranuclear copper(II) complexes bearing simultaneously carboxylate and aminoalcohol ligands which efficiently catalysed the oxidation of 2-aminophenol into the phenoxazinone chromophore.[13,16] An important observation was the pronounced enhancement of the reaction rate when a polynuclear catalyst was present in a solution. The preliminary theoretical assessment of the first step of the reaction (formation of aminophenoxyl radical) suggested that the role of dioxygen is likely in the formation of superoxo Cu^{II}–OO· species upon reaction with a reduced copper catalyst, rather than direct oxidation of aminophenolate substrate coordinated to the copper centre.[13] These results stipulated our further experimental and theoretical efforts on the investigation of PHS-like catalytic activity of copper complexes towards understanding the reaction mechanisms of aerobic oxidations of aminophenols, which is in line with our general interests in the chemistry and catalytic studies of polynuclear complexes.[11a,17] Herein we present the synthesis, crystal structures and characterization of bi- and trinuclear complexes, $[Cu_2(bae)_2(Cl)_2]$ (**1**), $[Cu_2(Hbae)_2(bae)_2](NO_3)_2$ (**2**) and $[Cu_3(Hbae)_2(bae)_2(dmba)_2](NO_3)_2$ (**3**), where Hbae is 2-benzylaminoethanol and Hdmba is 2,2-dimethylbutyric acid. The crystal structure of **2** has been reported previously.[18] All three compounds were found to show the phenoxazinone synthase mimicking activity towards aerobic oxidative coupling of 2-aminophenol and its derivatives. DFT/CASSCF theoretical calculations were performed to model the putative catalytically active species and differentiate the activities of substrates.

Results and Discussion

Synthesis and Spectroscopic Analysis

Complexes **1**–**3** were obtained through the self-assembly reaction of copper salts with a methanol solution of 2-benzylaminoethanol (Hbae) in the absence (for **1**) or presence (for **2** and **3**) of 2,2-dimethylbutyric acid (Hdmba) (Scheme 1). The reactions were initiated and brought to completion by heating (30–60 °C) and stirring in open air. At the end of reactions, blue-green solutions were obtained. Green-blue crystals of **1** suitable for the X-ray crystallographic study were formed within one day from the resulting solution without any additional procedures, while crystals of **2** and **3** grew within two weeks. Both complexes **2** and **3** can be obtained from the same reaction mixture, where the reaction temperature is the crucial factor that influences which compound is obtained. The higher temperature (60 °C) leads to the isolation of the complex **2**, while the lower one (30 °C) affords the complex **3** as the

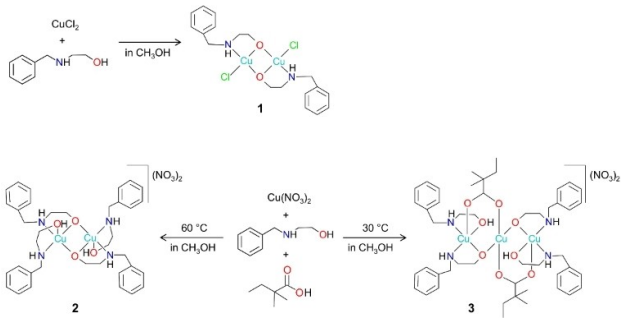

Scheme 1. Synthetic approach towards **1**–**3**.

reaction product. The lower yield of complex **2** in the latter case can be associated with the lower shift of the respective equilibria towards its formation. The synthesis of **2** can be reproduced in the absence of a carboxylic acid as reported elsewhere.[18] The general reactions of the overall formations of **1**–**3** can be written as follows, where the acids formed in the course of a reaction are captured by the bases (aminoalcohol and triethylamine) to form the respective salts:

$$2CuCl_2 + 2Hbae \rightarrow [Cu_2(bae)_2(Cl)_2] + 2HCl \quad (1)$$

$$2Cu(NO_3)_2 + 4Hbae \rightarrow [Cu_2(Hbae)_2(bae)_2](NO_3)_2 + 2HNO_3 \quad (2)$$

$$3Cu(NO_3)_2 + 2Hdmba + 4Hbae \rightarrow [Cu_3(Hbae)_2(bae)_2(dmba)_2](NO_3)_2 + 4HNO_3 \quad (3)$$

The IR spectra of **1**–**3** demonstrate complex patterns in the 400–2000 cm^{-1} region and confirm the presence of 2-benzylaminoethanolate in case of **1** and **2**, and the presence of both 2,2-dimethylbutyrate and 2-benzylaminoethanolate ligand in case of **3** (Figures S1–S3). The strong absorption peak at 3157 cm^{-1} in the spectrum of **1** and the peaks of medium intensity at 3185 and 3233 cm^{-1} (for **2**), and 3210 cm^{-1} (for **3**) were attributed to the ν(NH) frequencies of coordinated aminoalcohol ligand making strong N–H···Cl (for **1**) or N–H···O (for **2** and **3**) hydrogen bonds. The ν(CN) stretching vibration is observed in the 1065–1080 cm^{-1} region in the spectra of all compounds. The very strong band in the range 1200–1300 cm^{-1} (for **2** and **3**) splitted over many minor absorptions was assigned to ν(NO) vibration of the nitrate anions making different hydrogen bonds in the lattice. In the spectrum of **3**, the very strong bands at 1553 cm^{-1} and 1321 cm^{-1} (Figure S3) were attributed to the antisymmetric and symmetric COO^- stretching frequencies of 2,2-dimethylbutyrate acid, respectively.

The assignment of the sharp high-energy peak at 3157 cm^{-1} for **1** was confirmed by the DFT calculations of the frequencies at the composite r^2SCAN-3c level[19] using the crystallographic atomic coordinates with H atoms optimized (see below). The dimeric fragment containing four copper centres was selected to model the closest intermolecular hydrogen bonds (Figure S4 and S5). The ν(NH) frequency predicted for the H atoms

participating in the N–H···Cl bonding is 3290 cm^{-1} (experimental value is 3157 cm^{-1}). Remarkably, the predicted absorption of the N–H bonds not participating in the hydrogen bond in this model has negligible intensity at a slightly higher frequency (3408 cm^{-1}, Figure S4).

Crystal Structures

The single crystal X-ray diffraction analysis of the compound $[Cu_2(bae)_2(Cl)_2]$ (**1**) revealed that it is based on the centrosymmetric binuclear $\{Cu_2(\mu\text{-}O)_2\}$ core, where the copper(II) atoms are bound together by means of the μ-oxygen bridging atoms from 2-benzylaminoethanolate moieties (Figure 1). The deprotonated aminoalcohol ligands in **1** show bidentate N,O-donor coordination mode being responsible for the molecular structure type formation and for the metal ion charge compensation. The copper(II) cations in **1** have distorted square planar coordination environments with an O_2NCl donor set formed by oxygen and nitrogen atoms from 2-benzylaminoethanolate ligand and coordinated chloride ion. The Cu–O/N distances are in the range from 1.906(5) to 1.992(6) Å and Cu–Cl distance is 2.209(2) Å. The *cis* O/N–Cu–O/N/Cl bond angles vary from 84.4(2) to 101.94(18)° and *trans* O–Cu–N and O–Cu–Cl angles are from 158.4(2) to 169.70(17)°, respectively (Table S2). The Cu···Cu distance in the binuclear complex is 2.9883(18) Å. The strong intermolecular N–H···Cl hydrogen bonds with participation of the nitrogen atoms from aminoalcoholate ligands and coordinated chlorine atoms (Table S5) lead to the formation of the overall 1D supramolecular structure (Figure S6) in **1**. The binding energy of the intermolecular N–H···Cl hydrogen bond can be estimated from the electron density $\rho(\mathbf{r})$ at the respective bond critical point (Figure S5). The $\rho_{BCP}(\mathbf{r})$ value of 0.0185 a.u. can be converted[20] to the binding energy of −4.86 kcal mol^{-1}. Thus, the two hydrogen bonds between the neighbouring molecules of **1** have the total binding energy of −10 kcal mol^{-1} magnitude, which stipulate 1D packing in the solid state. The arrangement of the bulky substituents of the aminoalcoholate ligands hampers the formation of hydrogen bonding between adjacent supramolecular chains preventing subsequent increase of the dimensionality of the H-bonded polymer (Figure S6). The nearest non-bonded Cu···Cu separation within the supramolecular chain is 5.1038(11) Å.

The crystal structure of $[Cu_2(Hbae)_2(bae)_2](NO_3)_2$ (**2**) has been reported previously, showing the same topology of the coordination core but a slightly different geometry and the absence of positional disorder of the phenyl group.[18] Similarly to **1**, it features a binuclear molecular $\{Cu_2(\mu\text{-}O)_2\}$ core, but in case of **2** the whole core represents a crystallographically independent unit (Figure 2). The complex contains two 2-benzylaminoethanol ligands in the protonated form and the other two in the deprotonated one where all show bidentate (N,O) coordination (Table S3). The crystal structure of **2** has two crystallographically independent copper(II) atoms both of them with distorted square-pyramidal coordination environments with O_3N_2 donor sets formed by atoms from aminoalcoholate ligands. The basal Cu–O/N distances assume values in the range from 1.929(3) to 2.047(4) Å, while apical Cu–O bond lengths are 2.340(4) and 2.349(4) Å for Cu1 and Cu2, respectively (Table S3). The O–Cu–N_{trans} angles lie in the range 154.23(16)–177.97(13)°. The non-bonded Cu···Cu distance within the binuclear core is 2.9980(7) Å. The binuclear molecules in **2** are joined together by strong intramolecular hydrogen bonding of two types, O–H···O and N–H···O, involving oxygen and nitrogen atoms from aminoalcoholates and oxygen atoms from uncoordinated nitrate anions as well (Table S5), resulting in the formation of a 2D layer in **2** (Figures S8 and S9).

Crystallographic analysis shows that compound **3** consists of trinuclear centrosymmetric $[Cu_3(Hbae)_2(bae)_2(dmba)_2]^{2+}$ cationic molecules and two uncoordinated NO_3^- anions (Figure 3), linking the trinuclear units into the supramolecular polymeric chains by means of strong hydrogen bonding (Figures. S10 and S11). Two of aminoalcohol ligands in **3** remain protonated and other two are deprotonated revealing a bidentate (N,O) coordination, similar to that observed in **2**. The deprotonated 2,2-dimethylbutyrate ligands have the bidentate-chelating coordination mode and additionally join the neighbouring copper atoms in the consecutive way, thus serving for the metal ion charge compensation and strengthening the trimetallic mole-

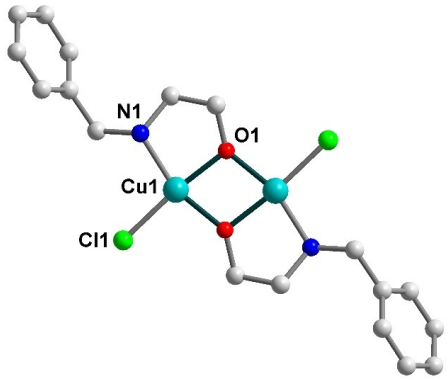

Figure 1. Molecular structure of **1** showing the numbering scheme of non-carbon atoms. Hydrogen atoms are omitted for clarity. Colour scheme: Cu, cyan; Cl, green; N, blue; O, red; C, grey.

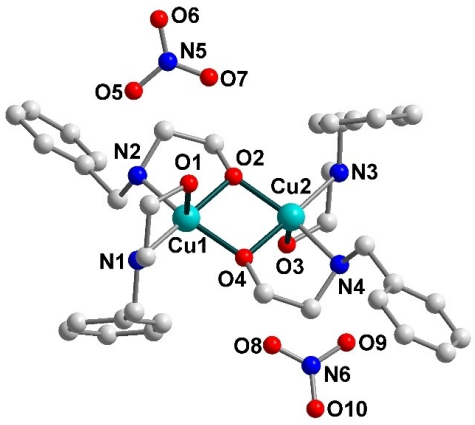

Figure 2. Molecular structure of **2** showing the numbering scheme of non-carbon atoms. Hydrogen atoms are omitted for clarity. Colour scheme: Cu, cyan; N, blue; O, red; C, grey.

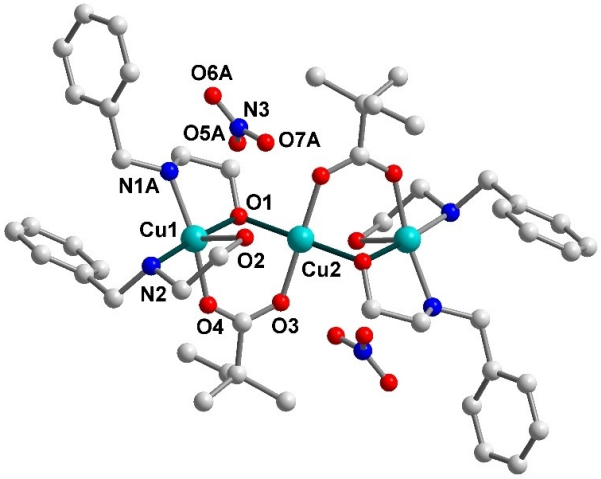

Figure 3. Molecular structure of 3 showing the numbering scheme of non-carbon atoms. Hydrogen atoms are omitted for clarity. Colour scheme: Cu, cyan; N, blue; O, red; C, grey.

cule. The distorted square-pyramidal coordination geometry around one of the two crystallographically independent copper atom, Cu1, is based on a O_3N_2 donor set which is formed by one oxygen and two nitrogen atoms from aminoalcoholate ligands and one oxygen from carboxylate [Cu1–O/N = 1.921(2)–2.038(3) Å] in the basal plane and one oxygen atom from the Hbae ligand [Cu1–O = 2.303(3) Å] at the apical position. The *cis* O–Cu1–O/N bond angles vary from 80.86(13) to 102.77(15)° and *trans* O–Cu1–N bond angles are 161.24(15) and 175.76(12) (Table S4). The second crystallographically independent copper atom, Cu2, has a distorted square planar coordination environment with an O_4 donor set formed by donor atoms from 2-benzylaminoethanolate and 2,2-dimethylbutyrate. The Cu2–O distances are 1.924(2) and 1.939(2) Å, while the *cis* O–Cu2–O bond angles vary from 88.84(11) to 91.16(11)° and *trans* O–Cu2–O angles are equal to 180.0°. The closest Cu···Cu distance within the trinuclear complex is 3.1318(5) Å. Similarly to **2**, the strong intramolecular H–bonding of O–H···O and N–H···O types, involving oxygen and nitrogen atoms from aminoalcoholates and oxygen atoms from NO_3^- anions is observed in **3** (Table S5). In contrast to supramolecular 2D layers in **2**, the formation of supramolecular 1D chains occurs in the case of **3** (Figure S10). The nearest non-bonded Cu···Cu separation between the trinuclear molecules within the supramolecular chain is 8.844(33) Å. It should be noted that according to Cambridge Structural Database (version 5.45)[21] the compound **3** is the first example of a transition metal mixed-ligand complex bearing simultaneously 2-benzylethanolaminate and 2,2-dimethylbutyrate ligands.

Catalytic Activity and UV-Vis Spectroscopy of 1–3

The coordination compounds **1**–**3** were studied as catalysts for the aerobic oxidative coupling of aminophenols into the phenoxazinone chromophore. The structure of the product chromophore depends on the presence and position of substituents. The unsubstituted 2-aminophenol (**I**) is known to form the phenoxazinone chromophore **P** which is the antibiotic Questiomycin A (Scheme 2).[22, 23] The substrates bearing the group R in the *ortho*-and *para*-positions relative to the amino group afford the "direct" isomer $\mathbf{P_1}$ and $\mathbf{P_3}$, while the sterical hindrance of the substituents in the *para*-position relative to hydroxo group is known[24] to produce the inverted chromophore $\mathbf{P_2}$ (Scheme 2). The chromophores $\mathbf{P_2}$ and $\mathbf{P_3}$ are not completely oxidized due to the impossibility of the final dehydrogenation step.[12a,c,24] The use of organic and inorganic (metal-based) oxidants under catalytic conditions may afford chromophores of unsymmetrical structures.[12c] In the present case of copper-catalysed aerobic oxidation, formation of the inverted isomer of unsubstituted chromophore **P** was excluded based on the TDDFT and STEOM-DLPNO-CCSD theoretical calculations of the UV-Vis absorption spectra (see the Supplementary Information, Scheme S1, Figure S12, Table S6).

The unsubstituted substrate **I** was used to study the catalytic behaviour of **1**–**3**. The reaction progress was monitored by measuring the intensity of the characteristic absorption band of the phenoxazinone chromophore[25] in the visible region (435 nm for 2-aminophenol substrate, **I**). The absorptions were converted to the concentrations of the product (phenoxazinone chromophore) through the extinction coefficients known from literature[25–26] and confirmed herein (Table S6). The typical UV-Vis spectra observed during the catalytic reaction with $[\mathbf{I}]_0 = 10$ mM and $[\mathbf{1}]_0 = 0.084$ mM are depicted in Figure 4. The initial reaction rate, W_0, was calculated using the extinction coefficient $\varepsilon = 2.4\times10^4\ M^{-1}\ cm^{-1}$ (for **I**)[16,25] resulting in $W_0 = 1.1\times10^{-8}\ M\ s^{-1}$. The complexes **2** and **3** tested under the same conditions gave slightly lower rates of 7.3×10^{-9} and 8.5×10^{-9} M s^{-1}, respectively.

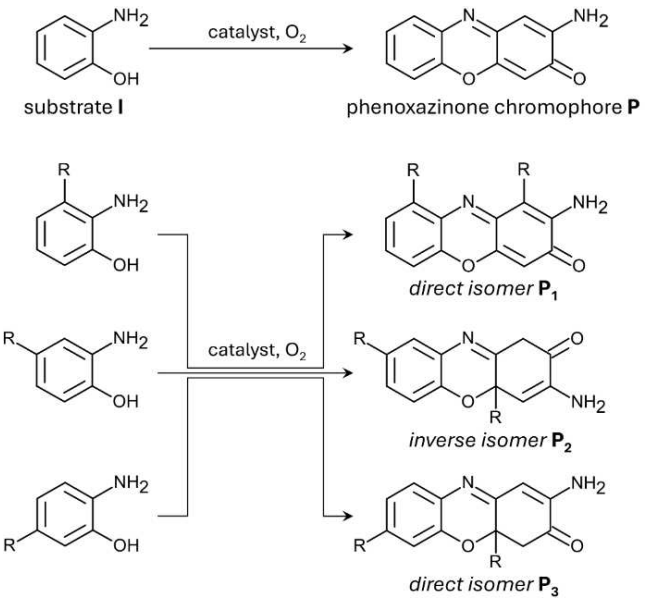

Scheme 2. Catalytic oxidative coupling of unsubstituted 2-aminophenol (**I**) as well as its derivatives, and structures of the respective phenoxazinone chromophores depending on the position of the substituent R.

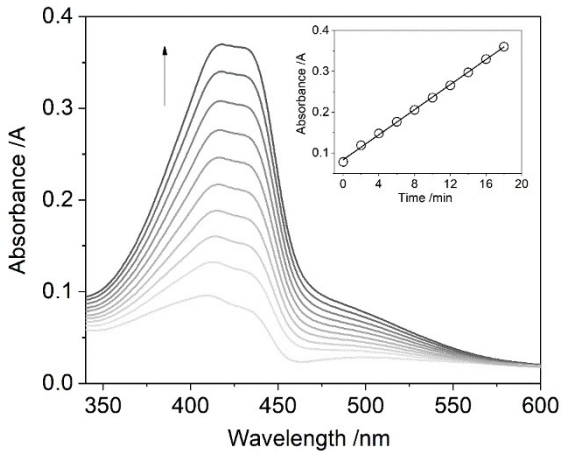

Figure 4. Increase of the phenoxazinone chromophore absorption over time (2 min interval) in the oxidation of **I** (0.01 M) catalysed by **1** (0.084 mM) in CH_3OH at room temperature. Inset shows the increase of 435 nm absorption with time.

The W_0 *vs.* $[cat]_0$ dependencies for **1**–**3** are plotted in Figure 5. Considering the possible equilibria between different polynuclear compounds in solution,[16] here and onward the total concentration of copper $[Cu]_0$ was used as the catalyst concentration. The W_0 *vs.* $[Cu]_0$ dependencies have linear behaviour in the 0–0.6 mM concentration range (the highest $[Cu]_0$ for **1** is limited by its low solubility in methanol) indicating no aggregation of the catalytically active species in solution in the range studied. The catalysts **2** and **3** exhibit similar behaviour with the maximum reaction rate of 2.3×10^{-8} M s^{-1} (Figure 5). The TOF for both **2** and **3** does not show significant variations (3.6×10^{-5}–5.1×10^{-5} s^{-1}) in the studied range of concentrations. In contrast, the growth of the catalytic activity of **1** is more acute, reaching TOF = 9.6×10^{-5} s^{-1} for $[Cu]_0$ = 0.034 mM and maximum W_0 of 6.4×10^{-9} M s^{-1} for $[Cu]_0$ = 0.134 mM. The investigation of the reaction rate at higher concentrations is limited by the insufficient solubility of **1** in methanol.

The linear W_0 *vs.* $[Cu]_0$ dependence for **1** also indicates that no interaction occurs between copper species when $[Cu]_0 < 10^{-4}$ M. For comparison, the tetranuclear complex $[Cu_4(bae)_4(va)_4]\cdot H_2O$ (where Hva = valeric acid) exhibits a non-linear behaviour even at the $[Cu]_0 < 0.5$ mM concentrations due to the equilibria between the tetra- and binuclear coordination compounds in solution.[16] However, the identical W_0 *vs.* $[Cu]_0$ dependencies (Figure 5) for the bi- and trinuclear compounds **2** and **3**, respectively, indicate that their catalytic behaviours are equal, and the polynuclear cores are likely to decompose to mononuclear compounds in diluted solutions. Such behaviour is expected for polynuclear coordination compounds with flexible mono- and bidentate aliphatic ligands,[16] where the components (ligands and metals) form a dynamic combinatorial library[27] in solution. In this way the starting coordination compound acts as a pre-catalyst. The dependence of the reaction rate on the substrate concentration for catalyst **1** and 2-aminophenol substrate (**I**) was found to be linear in the 6–54 mM range of concentrations (Figure 6). Therefore, the overall rate-law expression can be written as $W = k$[catalyst][substrate].

It is important to note that metal salts often used as catalysts for comparative purposes may give misleading results due to aggregation of metal species in solution. Such behaviour of copper *e.g.* chloride was documented recently by us for the same PHS-like reaction[16] as well as by other groups for other processes.[28] This uncertainty and potentially higher activity of polynuclear compounds or oxide nanoparticles could result in significant overestimation of reaction rates when using metal salts as (pre)catalysts, thus we would like to refrain from making such comparisons in the present case.

The UV-Vis spectra of catalytic solutions recorded at the first minutes of reaction exhibit an absorption band around 600 nm. The intensity of this band was found to be higher for the cases of lower catalyst/substrate ratio (i.e. higher catalyst loading). Visually, the light-yellow methanol solution of equimolar amounts of the substrate **I** and complex **3** quickly becomes dark grey blue after mixing the reagents (0.25 mM final concentrations), then undergoing gradual change of the colour to yellow brown upon accumulation of the phenoxazinone

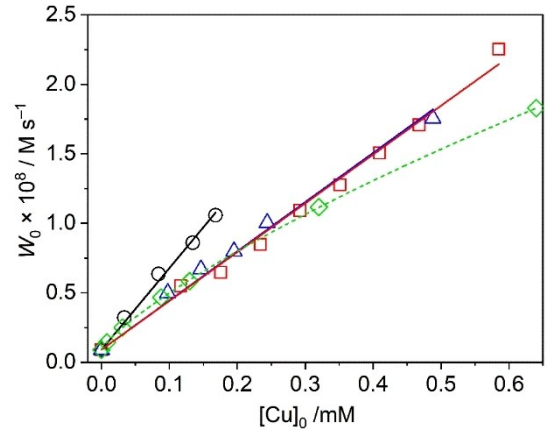

Figure 5. W_0 *vs.* $[Cu]_0$ dependencies for **1**–**3** (**1**: black circles; **2**: blue triangles; **3**: red squares) and $[Cu_4(bae)_4(va)_4]\cdot H_2O$ (green rhombs).

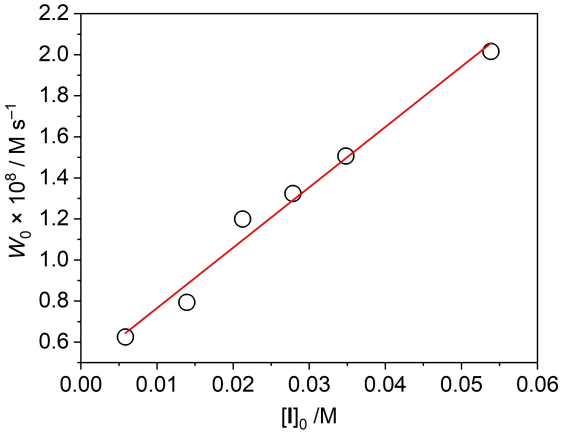

Figure 6. W_0 *vs.* $[I]_0$ dependence for **1** ($[Cu]_0$ = 0.17 mM). Black circles are experimental data, red solid line is a linear fit.

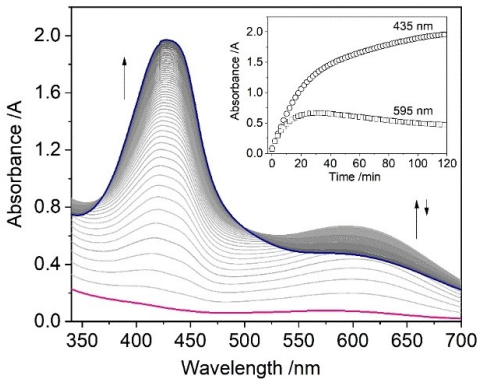

Figure 7. Evolution of the UV-Vis spectra with time (2 min interval) of the methanol solution of **I** and **3**, where $[I]_0 = [Cu]_0 = 0.25$ mM. The inset shows the change of absorbance intensity with time at 435 and 595 nm.

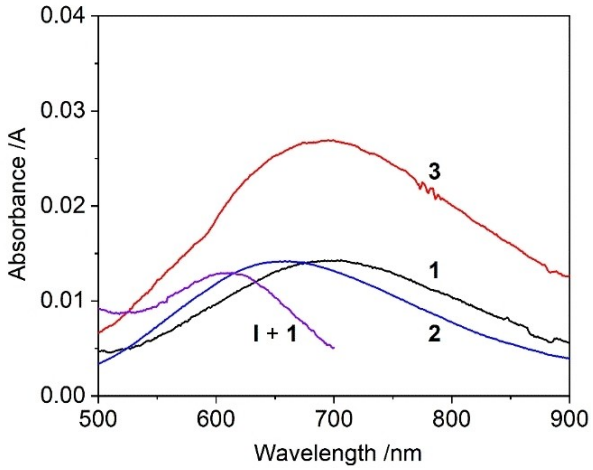

Figure 8. UV-Vis spectra of the complexes **1**–**3** in methanol ([Cu] = 0.1 mM). The purple line shows the spectrum of **I** : **1** equimolar mixture in methanol with $[I]_0 = [Cu]_0 = 0.085$ mM (Figure 9), normalized to 0.1 mM, measured immediately after mixing the components.

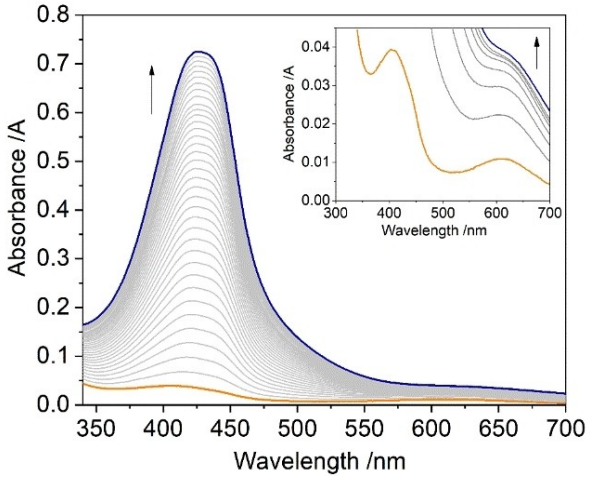

Figure 9. Evolution of the UV-Vis spectra with time (2 min interval) of the methanol solution of **I** and **1**, where $[I]_0 = [Cu]_0 = 0.085$ mM. The inset shows the change of evolution of absorbance in 300–700 nm region (8 min interval).

chromophore. The evolution of the respective UV-Vis spectrum is shown in Figure 7, where an intense absorption band at 595 nm is seen with the maximum absorption at 30 min. The wavelength of this absorption is shorter than the d-d absorptions of pure complexes **1**–**3** in methanol, which constitute 700, 660 and 695, respectively (Figure 8). The complex **1** treated with equimolar concentration of the substrate **I** in methanol exhibits the hypsochromic shift down to 610 nm. With the low concentration of **1** (0.085 mM) the decay of the 610 nm absorption band is hidden by the strong absorbance of the phenoxazinone chromophore (Figure 9). The reaction rate of phenoxazinone chromophore accumulation exhibited by the $[I]_0 = [Cu]_0 = 0.085$ mM (100 mol % catalyst loading) mixture is 1.1×10^{-8} M s^{-1}, being almost equal to that for 1.7 mol % loading.

Catalytic Behaviour of Substituted Aminophenols

To investigate the influence of the substituents on the reaction rate, several isomers containing methyl-, nitro- and chloro-substituents in the aminophenol core have been studied (Figure 10). The molar extinction coefficients were obtained from literature and/or confirmed herein (Figuress S19-S22, Table S11). The catalyst-free reaction rates of the methyl-derivatives **II**–**IV** at 5 mM concentration were found to be quite different. Substrate **II** exhibited the reaction rate of 8.4×10^{-10} M s^{-1}, slightly higher than that found for unsubstituted 2-aminophenol (3.6×10^{-10} M s^{-1} for 5 mM initial concentration).

The aminophenol with the methyl group in *para*-position relative to hydroxyl group (**III**) revealed rather low reactivity with the reaction rate of 1.8×10^{-10} M s^{-1}. In contrast, the 6-amino-*m*-cresol **IV** demonstrated an almost one order higher reaction rate of 2.2×10^{-9} M s^{-1}. The choro-derivative **VIII** showed significant difference between the initial and linear reaction rates. While the initial region demonstrates a rather high rate of 3.0×10^{-8} M s^{-1}, after 40 min it slows down to 3.4×10^{-11} M s^{-1}. The catalyst-free reaction rates of nitro-aminophenoles were found to be too small for their reliable estimation, also leading to difficulties in the determination of the extinction coefficients of the respective chromophores. Furthermore, the nitro-substrates exhibit strong absorbance in the visible region (Figures S14 and S15) at the wavelength close to that expected for the respective phenoxazinone chromophore. The phenoxazinone chromophore products were not isolated in the present investigation which is focused on the catalytic study of the

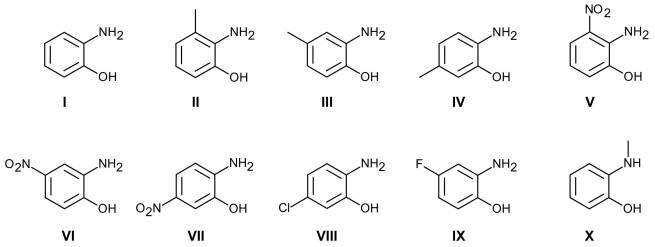

Figure 10. 2-aminophenol derivatives studied in this work.

initial reaction rates. Some of the products **I**–**X** are known to be isolated and spectroscopically characterized elsewhere.[12a,24]

Reaction rates found for aerobic oxidations of **I**–**X** catalysed by **1** (Figure S29) followed the tendencies found for the catalyst-free reactions. Oxidation of the unsubstituted substrate **I** (5 mM) in the presence of **1** ($[Cu]_0 = 0.17$ mM) resulted in the reaction rate W_0 of 7.9×10^{-9} M s^{-1}. This rate is almost equal to that exhibited for $[\mathbf{I}]_0 = 10$ mM (8.0×10^{-9} Ms^{-1}), indicating no significant dependence of the reaction rate on substrate concentration in the range studied. Surprisingly, the oxidation rate of 2-amino-*m*-cresol (**II**) was not improved by the presence of a catalyst, as evidenced by the reaction rate $W_0 = 6.3\times10^{-10}$ M s^{-1}, while **III**, **IV** and **VIII** demonstrate significant increase of the oxidation rate due to the catalytic effect of **1** ($W_0 = 1.1\times10^{-8}$, 5.8×10^{-8} and 2.7×10^{-9} M s^{-1}, respectively, using $[substrate]_0 =$ 5 mM and $[Cu]_0 = 0.17$ mM).

The nitro-substituted substrates **V**–**VII** showed very low rates in the presence of a copper catalyst as well as in the catalyst-free reaction and considered to be inactive herein. The high inertness of the nitro-substituted 2-aminophenols was observed earlier.[12c] Moreover, modelling of the phenoxazinone chromophore structures at the TPSS/def2-TZVP level revealed that the $\mathbf{P_{VI}}$ product is not stable and undergoes elimination of NO_2^- group from the main chromophore structure forming a salt (Scheme S2), as evidenced by the respective d(C···N) separation of 2.497 Å (see the Supplementary Information).

The fluoro-substitute substrate **IX** (Figure 10) shows the highest reaction rate among the substrates studied of 1×10^{-7} M s^{-1} (Figure S29). The amino-substituted substrate **X** was studied for comparative purposes, while the formation of a complete phenoxazinone chromophore is not expected for this substrate due to the blocked position of the amino group. The catalytic reaction of **1** with 30-fold excess of **X** gave an increase of the absorbance at 340 nm (Figure S15). DFT modelling of the possible products as well as their absorption spectra resulted in the two stable structures having the predicted absorption maxima at 315 and 294 nm, being at higher energies than that calculated for the non-substituted phenoxazinone chromophore (386 nm; Table S7). Considering the slight overestimation of excited states energies by the chosen TDDFT level PBE0/aug-cc-pVDZ, one can assign the phenoxazinone models $\mathbf{P_{X\text{-}A}}$ and $\mathbf{P_{X\text{-}B}}$ (Figure S14) to the experimentally observed absorption spectra (Figure S15).

Formation of the phenoxazinone chromophore $\mathbf{P_I}$ was confirmed by its EI-MS spectrum where the molecular ion peak at 212 *m/z* as well as the characteristic spectral pattern[16] are observed at the GCMS chromatogram recorded after 4 h time (Figure S18). The chromatogram of the reaction using substrate **II** showed two peaks (Figure S19) that can be assigned to the final product $\mathbf{P_{II}}$ (240 *m/z*) as well as its hydrogenated intermediate (242 *m/z*). The GCMS chromatograms of the reactions starting from substrates **III** and **VIII** did not reveal detectable peaks due to low to moderate activity of the respective substrates as well as limitations of gas chromatography for the detection of large polar compounds (Figure S20 and S22). In contrast, the chromophore $\mathbf{P_{IV}}$ was clearly detected by the presence of a distinct molecular ion peak at 240 *m/z* (Figure S21). The EI-MS spectral patterns of $\mathbf{P_{II}}$ and $\mathbf{P_{IV}}$ are close, indicating similar decomposition pathways of the respective molecular radical cations formed upon the electron impact. The chromatogram recorded for the fluoro-substituted substrate **IX** revealed two peaks having the largest *m/z* values of 230 and 234 *m/z* (Figure S23) which is lower than expected for the molecular ion of $\mathbf{P_{IX}}$ or $\mathbf{P_{IX\text{-}inv}}$ of 250 *m/z*.

To confirm the assignment of the $\mathbf{P_{IX}}$ and $\mathbf{P_{IX\text{-}inv}}$ spectra to the respective phenoxazinone chromophore products, the theoretical calculations of the EI-MS spectra of $\mathbf{P_{IX}}$ and $\mathbf{P_{IX\text{-}inv}}$ at the semi-empirical GFN2-xTB level implemented in the QCxMS package were performed. For both $\mathbf{P_{IX}}$ and $\mathbf{P_{IX\text{-}inv}}$ structures the predicted spectra unambiguously show strong suppression of the molecular ion peak intensity which has less than 1% intensity in the case of $\mathbf{P_{IX}}$ (Figures S25 and S26), where the predicted 100% intensity peaks for $\mathbf{P_{IX}}$ and $\mathbf{P_{IX\text{-}inv}}$ are $[M - F]^+$ at 231 *m/z*. The peak at 230 *m/z* in the experimental spectrum of $\mathbf{P_{IX}}$ is thus can be interpreted as $[M - HF]^+$. The second largest peak at 203 *m/z* in the spectrum of $\mathbf{P_{IX}}$ (Figure S25) is observed in the theoretical fragmentation pattern, but with very low intensity of 2%. While the present semi-empirical calculations succeeded in predicting the low intensity of the molecular ion peaks, prediction of further fragmentation appears to be a challenge. To confirm the correctness of a molecular ion peak intensity prediction, the calculations at the same level were performed for the chromophore $\mathbf{P_I}$ having the well-established EI-MS spectrum. The 100% intensity peak in the theoretical EI-MS spectrum of $\mathbf{P_I}$ is a molecular ion at 212 *m/z* with the subsequent fragmentation to 184 and 171 *m/z* (Figure S24). While the latest value is absent in the experimental spectrum (Figure S18), the $[M]^+$ and $[M - CO]^+$ predicted peaks (212 and 184 *m/z*) agree with the experimental data. Therefore, the theoretical predictions of the low intensities of the molecular ion peaks for $\mathbf{P_{IX}}$ and $\mathbf{P_{IX\text{-}inv}}$ were considered reliable.

General Mechanistic Considerations

Formation of an aminophenoxyl radical **I·**, which can be viewed as activation of the substrate, is known to be the rate-limiting step towards the phenaxonizonone chromophore (Scheme 3).[29] Once the aminophenoxyl radical is formed, the mechanism proceeds through its further oxidation to the imino-quinone intermediate which undergoes Michael addition reaction with further oxidation towards the final phenoxazinone chromophore.[1c,5b,c,12b,29] The oxidation reaction can be initiated by free radicals. For example, the TEMPO radical is known to enhance the reaction rate of 2-aminophenol oxidation due to its independent action as a catalyst[16,29] Participation of metal-containing catalysts in the steps after formation of imino-quinone intermediate was proposed in several cases.[25,30] In the

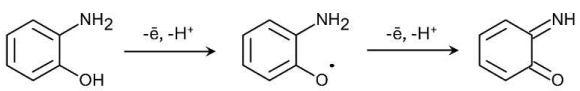

Scheme 3. Oxidation of 2-aminophenol to the respective imino-quinone.

presence of a copper catalyst and air dioxygen, the accelerated oxidation of aminophenol can be achieved upon its interaction with copper species. Another common mechanistic explanation is the aerobic oxidation of aminophenol coordinated to the metal centre,[4a,5a,b,9c,10a,31] where the aminophenol-metal complex assemblies were detected by ESI-MS, EPR and other spectroscopies. One has to note, however, that EPR of polynuclear systems can be silent in the common X-band mode, in this way giving a false-negative result. Furthermore, the EPR search for short-lived organic radicals in the presence of EPR-active copper compounds is a rather tricky task. In turn, the ESI-MS spectroscopy of labile coordination compounds may distort the composition of a solute due to specific reactions known to proceed in the ESI-MS ionization chamber.[32] Thus, in the present case we rely on the kinetic and theoretical data and focus on the copper-catalysed formation of an aminophenoxyl radical through theoretical studies.

Hydrogen peroxide is presumed to be formed in the catalytic cycle, but its detection under the conditions of experiment is a great challenge because of its low concentration and expected high catalytic Fenton-like and/or catalase-like activity of copper compounds towards the fast decomposition of H_2O_2. Due to these circumstances, detection and quantification of hydrogen peroxide was not conducted in the present study.

The dissolution of air O_2 was not expected to be a rate-limiting step based on the following considerations. The solubility of O_2 in methanol at room temperature is rather high, ca. 10 mM.[33] Hence, the amount of O_2 dissolved in the reaction mixture is sufficient to completely transform ca. 7 mM of aminophenol substrate to phenoxazinone chromophore, what is comparable or exceeds the concentrations typically used in the present investigation (ca. 0.1–10 mM). The rate dependences on the O_2 concentration for this type of reaction have been studied earlier,[34] always showing linear W_0 *vs.* $[O_2]_0$ plots regardless other conditions and even for the catalytic processes with high concentration of a substrate (up to 50 mM).

Despite it is known that copper superoxo species can abstract H atom from phenols with formation of phenoxyl radicals,[35] there are still very little experimental or theoretical efforts done towards characterization of the respective process in the course of phenoxazinone synthase-like catalytic activity. Participation of Cu^{II}–OO· species can be understood if one considers the reaction of $^3O_2$ with Cu(I) species appearing as a part of the catalytic cycle. Finally, Cu(II) coordination compounds are known to oxidize aminophenol in the absence of air,[16] eventually leading to the formation of the final product, phenoxazinone chromophore. Thus, both these reactions can constitute a closed catalytic cycle (Scheme 4).

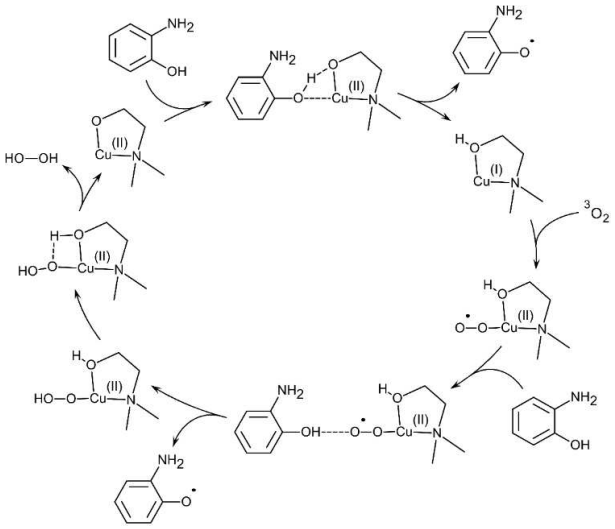

Scheme 4. Putative mechanism of aminophenoxyl radical formation.

Electronic Structure of the Model Superoxo Copper Complex

Formation of copper superoxo Cu^{II}–OO· intermediates is known for copper-mediated aerobic oxidations upon reaction of Cu^{I} species with molecular oxygen.[36] In the present case, the simplified mononuclear superoxo copper complex **A** with N-methylethanolamine (HL), acetate and methanol ligands, $[Cu^{II}(HL)(OAc)(CH_3OH)O_2]$, was used to facilitate the calculations. The mononuclear structure was selected due to the possible degradation of polynuclear species in diluted solutions,[16] which agrees with the identical W_0 *vs.* $[Cu]_0$ plots for **2** and **3** (Figure 5). Another reason for assuming a mononuclear structure for computational studies is the size of the system: calculation of reaction pathways for a large polynuclear compound is computationally expensive, especially for the search of transition state(s) and estimation of the vibrational energy.

It is assumed that the type of mechanism remains the same for other (larger) catalysts. The carboxylate (acetate) ligand was chosen to saturate the coordination environment of copper. Optimization of the model compound **A** at the TPSS/def2-TZVP level using C-PCM (methanol) solvation model resulted in the distorted octahedral geometry, typical for Cu(II) centre having $S = 1/2$ spin state (Figure 11). The meta-GGA TPSS functional without involvement of exact Hartree-Fock exchange was chosen due to the possible contribution of a multireference character of the model. The optimized structure features the Cu–O(N) distances in the basal plane ranging from 1.969 (for coordinated O_2 molecule) to 2.092 Å, while the apical distances constitute 2.397 and 2.654 Å. The angle Cu–O–O is 116.05°, which is close to reported values of 113° in superoxo copper complexes.[36a]

The diradical ground state of $^3O_2$ molecule is expected to result in the triplet ground spin state of the Cu^{II}–OO· moiety in **A**, where one electron is located on the copper atom and other one is distributed over the O_2 fragment. The DFT spin density obtained from the unrestricted SCF calculations (TPSS/def2-TZVP) is shown in Figure 11, where it indicates the involvement of both oxygen atoms as well as the copper centre. The broken symmetry (BS) calculations at the same theory level predict the ferromagnetic ground spin state with the BS state 786.8 cm^{-1} above it. The α orbital of the unrestricted corresponding (UCO) molecular orbital with overlap $S = 0.00518$ shows that the

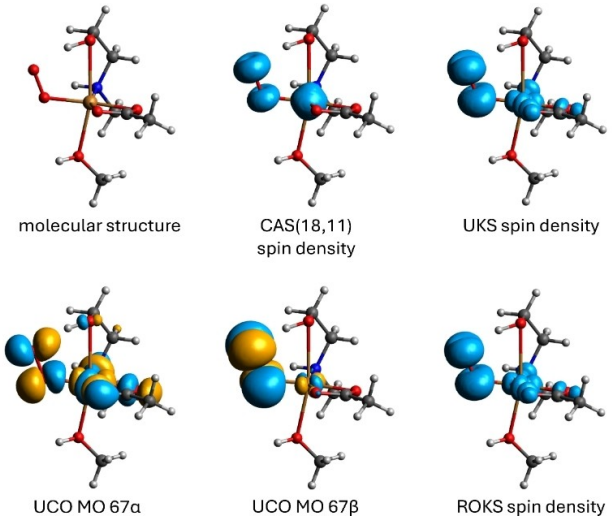

Figure 11. Structure of the model copper superoxo compound [Cu^{II}-(HL)(OAc)(CH_3OH)O_2] (**A**), optimized at the TPSS/def2-TZVP/C-PCM(methanol) level, and isosorfaces of spin densities and unrestricted corresponding orbitals (UCO) calculated at different levels.

unpaired electrons of the high-spin state are located at the antibonding π* molecular orbital of oxygen atoms and d_{x2-y2} orbital of copper atom. This distribution agrees with spin density and orbital populations obtained from the restricted open-shell DFT calculations (ROKS, Figure 11). The latter predicts two singly occupied orbitals (SOMOs) with 0.36 eV of difference, where the low-lying SOMO is constructed of 89% of p_y atomic orbitals of oxygen atoms. The HOMO-$SUMO_1$ and $SOMO_2$-LUMO gaps are 0.20 and 0.15 eV.

The state-averaged CAS(18,11)/NEVPT2 active space calculations involving five copper d-orbitals and six dioxygen p-orbitals indicated the triplet (biradical) ground spin state with the first singlet state lying 418.7 cm^{-1} above when considering 8 roots for every multiplicity (425.2 cm^{-1} for 14 and 10 roots for singlet and triplet state, respectively). The set of molecular orbitals is similar to that expected for dioxygen molecule with two orbitals significantly mixed with d_{x2-y2} ones of the copper atom (Figure 12). The ground state is constructed of one dominant configuration (65.2%) with two unpaired electrons located at the π^*p_y and d_{x2-y2}-p_xp_z orbitals, while the remaining configurations share the second unpaired electron over the d_{x2-y2}-π^*p_x and d_{z2} orbitals.

Not surprisingly, the composition of the ground state depends on the number of excited states involved into the CAS calculation. The same active space shared over [14,10] roots results in 84.0% of the same ground state configuration. These observations suggest that the ground state is in fact not a multireference one and the observed mixing of configurations is rather a result of the insufficiently precise description of electronic structure of **A** by the CAS(18,11) active space. The state-specific calculation confirmed that the triplet ground state is completely single-reference.

Reactivity of the Model Complex A towards H Atom Abstraction

Interaction of the model compound **A** with the molecule of 2-aminophenol, **I**, is expected to proceed through the formation of a hydrogen bond between the hydroxyl group and

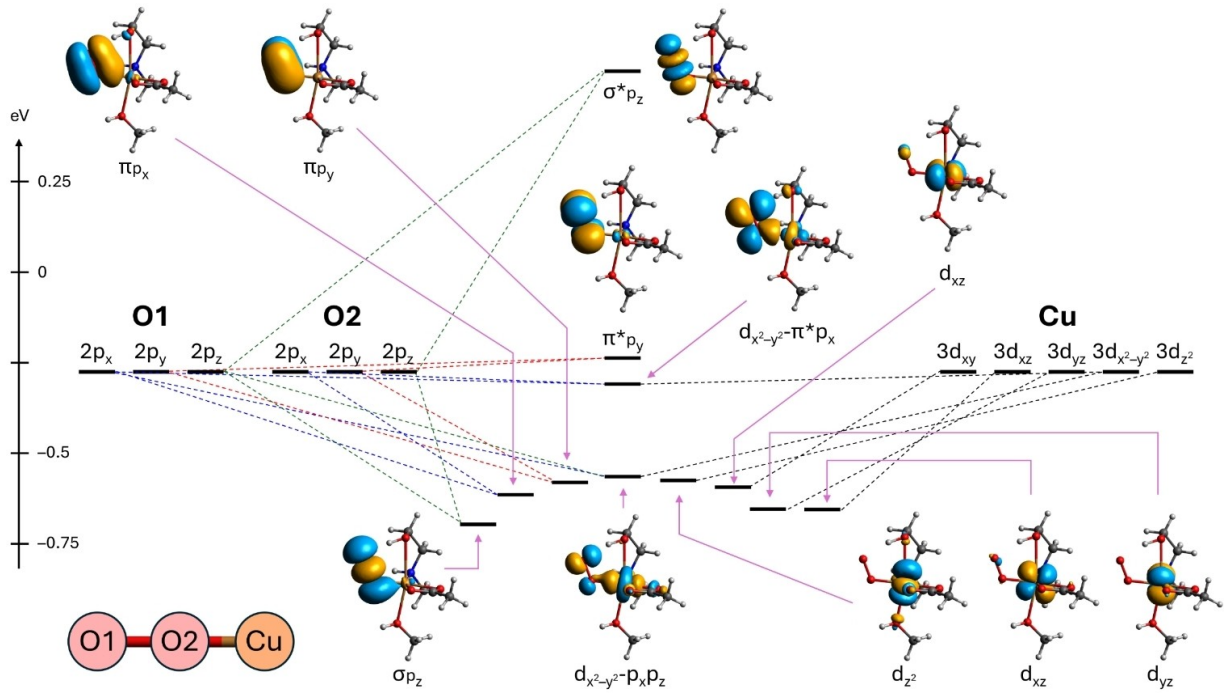

Figure 12. Energy diagram and isosurfaces of the active space molecular orbitals for the CAS(18,11) calculation on the model compound [Cu^{II}-(HL)(OAc)(CH_3OH)O_2] (**A**). The energies of starting atomic orbitals are not in scale.

coordinated O_2 molecule, where the aromatic ring forms broad non-covalent interactions with aminoalcohol part of **A**. To confirm such assumption, the search for possible conformations of the {**A**+**I**} assembly was performed employing the GFN-FF force field model implemented in the CREST package. Screening of 966 configurations resulted in a single stable conformation which corresponds to the one described above.

The energy profile of the H-abstraction from **I** by **A** was calculated at the TPSS/def2-TZVP//ωB97M-V/def2-QZVPPD level (Figure 13). The choice of the range-separated DFT functional for correction of electronic energy was governed by its sufficient quality-to-costs ratio. The energy profile obtained at this level for the catalyst-free oxidation of **I** is similar to that obtained previously at the B3LYP/ma-def2-TZVP//DLPNO-CCSD(T)/ma-def2-TZVPP level.[13] In the present case, the correction at the DLPNO-CCSD(T)/cc-pVTZ level[37] gave slightly different energies, but at approximately ten times higher computational costs. The RI-SCS-MP2/cc-pVTZ method[38] was also tested but, in some cases, found to give unreliable results with significantly overestimated energy differences. Notably, the electronic energies predicted by the meta-GGA TPSS functional show a very large deviation from the range-separated DFT and post-HF methods, predicting almost no barrier of less than 2 kcal mol^{-1} (Table S8). The latter results are not surprising as the estimation of absolute electronic energies is a weak point of non-hybrid DFT functionals.

The hydrogen atom transfer from the hydroxyl group of aminophenol to the oxygen atom of coordinated O_2 molecule proceeds through a single transition state. The reaction starts with formation of the supramolecular intermediate ^{3}**Int$_a$** (^{3}**Int$_{Ia}$** for the case of **I**). Despite the binding energy of −9.40 kcal mol^{-1}, the overall Gibbs free energy change indicates that the ^{3}**Int$_{Ia}$** intermediate is 4.8 kcal mol^{-1} less favourable than the sum of its components. The transition stage ^{3}**TS$_{Ia}$** shows the barrier of 16.7 kcal mol^{-1} relative to ^{3}**Int$_{Ia}$** (21.5 kcal mol^{-1} relative to **A**+**I** sum) at 298.15 K, indicating the feasibility of the reaction. The after-barrier intermediate ^{3}**Int$_{Ib}$** is equal to the ^{3}**Int$_{Ia}$** (0.05 kcal mol^{-1} of difference), while disassembly ^{3}**Int$_{Ib}$** into the aminophenoxyl radical and Cu^{II}–OOH complex **AH** results in further decrease of free Gibbs energy down to 2.0 kcal mol^{-1} relative to the sum of Gibbs energies of starting **A** and **I** components.

The model with chloride ligand instead of acetate one, [Cu^{II}(HL)Cl(CH$_3$OH)O$_2$] (**A^{Cl}**), was explored for comparative purpose. Optimization of the **AI^{Cl}** resulted in the distorted trigonal bipyramidal environment around the copper centre with the angle Cu–O–O being slightly higher (120.64°) than that for the model **A**. The free Gibbs energy of the {**A^{Cl}**·**I**} assembly (intermediate ^{3}**Int$_{Ia}$**) formation is 4.9 kcal mol^{-1}, being very close to that obtained for the model catalyst **A**. However, the activation energy $\Delta G^{\ddagger}$ exhibited by **A^{Cl}** for the oxidation of unsubstituted aminophenol was found to be notably smaller (17.3 kcal mol^{-1}; Table S9) than that estimated for the acetate model **A** (21.5 kcal mol^{-1}). This observation agrees with the higher activity of the complex **1** (Figure 5) which bears chloride ligand instead of the acetate one.

The reaction mechanism was found to be independent of the substituents in the aminophenol aromatic ring except for the substrate **III**, for which an optimization of the ^{3}**Int$_{IIIb}$** structure always leads to decoordination of the methanol molecule in this way resulting an underestimated energy. The same behaviour was observed for the substrate **X**, for which the steric repulsion between the catalyst and N-methyl group results in the shift of the substrate molecule compared to the

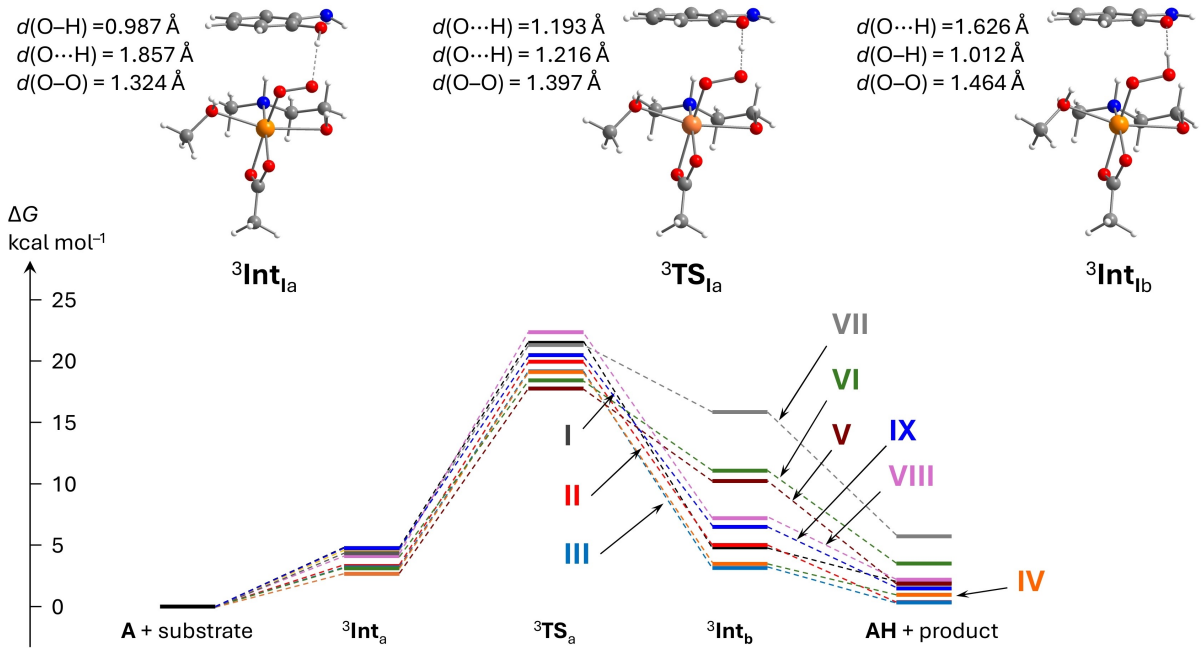

Figure 13. Free energy profile and geometries of the intermediates for the H atom abstraction from 2-aminophenol substrates **I**–**IX** by the model copper superoxo complex [Cu^{II}(HL)(OAc)(CH$_3$OH)O$_2$] (**A**) calculated at the TPSS/def2-TZVP//ωB97M–V/def2-QZVPPD level. The Gibbs energy of ^{3}**Int$_{IIIb}$** intermediate is underestimated due to the decoordination of the methanol ligand.

other substrates. The spread of the energy barriers in all cases was found to be relatively small (Table S8). The principal difference between the energy profiles of **I**–**IX** is the level of the ^{3}**Int$_b$** intermediate which has strong influence on the rate of the inverse reaction ^{3}**Int$_b$** → ^{3}**TS$_a$** → ^{3}**Int$_a$**. The rate constant of a reaction is in exponential dependence on its activation barrier $\Delta G^{\ddagger}$, according to the Eyring equation. Considering the reversibility of the H-abstraction process, the twice lower ^{3}**TS$_a$** – ^{3}**Int$_b$** barrier for **V**–**VII** should result in several orders increase of the inverse rate constant k_i, leading to significant hampering of the overall reaction due to the prevalence of the inverse reaction over the direct one. The fact that the nitro-substrates **V**–**VII** are unreactive towards both copper-catalysed and catalyst-free oxidations suggests that the explanation of their low reactivity could be in the destabilization of the respective nitro-aminophenoxyl radicals.

The vertical and adiabatic electron affinities of **V**–**VII** radicals were found to be ca. 13 kcal mol^{-1} (ca. 0.6 eV) higher than those for other studied aminophenoxyl radicals (Table S10), clearly indicating their higher reactivity in the processes involving an electron abstraction. This effect can be associated to the electron configuration of the nitro group which partially loses its resonance stabilization upon elimination of one electron from the whole molecule.

The Catalyst-Free Process

The mechanism of a catalyst-free oxidation of aminophenols with molecular dioxygen is more complicated than the copper-catalysed one due to the significant conformational flexibility of the {substrate·$^3O_2$} assembly, as well as of the final {product·OOH} one. The search for possible configurations through the GFN-FF force field approach implemented in CREST resulted in seven possible configurations for the {**I-radical**·OOH} assembly and more than one thousand for {**I**·$^3O_2$} one. Visual inspection of seven configurations for both reactant and product showed multiple geometrical arrangements, from which the lowest one presumes interaction of $^3O_2$ molecule with oxygen atom of **I** and an aromatic H atom (Figure 14). The respective planar configuration was studied earlier by us,[13] resulting in the barrier of 28.7 kcal mol^{-1} and low stabilization of the product assembly (25.9 kcal mol^{-1} relative to the sum of free Gibbs energies of **I** and $^3O_2$). This $\Delta G^{\ddagger}$ is close to that obtained here for metal-catalysed gap G(^{3}**TS$_{Ia}$**) – G(**A** + **I**)) (Figure 13, Table S8). From the multiple configurations of the {**I-radical**·OOH} assembly it is obvious that the true catalyst-free reaction may proceed in several configurations having different geometries of transition states. The preliminary calculations of the nitro-substrates **V**–**VII** revealed $\Delta G^{\ddagger}$ barriers up to 28.1 kcal mol^{-1}, which are compatible to that for **I**. Therefore, the principal difference in the reaction rates of oxidation of **I**–**VIII** is in the energies of radical species and their electron affinities (Table S10) rather than in the transition states.

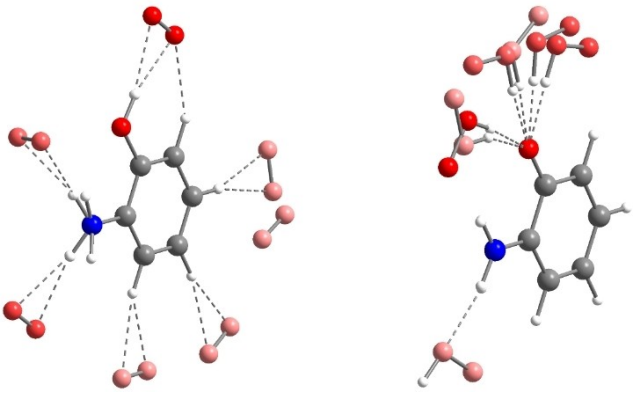

Figure 14. Conformational analysis of the {**I**·$^3O_2$} and {**I-radical**·OOH} assemblies (left and right, respectively) performed at the CREST/GFN-FF level. Lighter red colour of oxygen atoms corresponds to higher energy of the respective $^3O_2$ or HOO· position.

Interaction of 2-Aminophenol with 1 and with Model Complex B

Apart from the O_2-mediated oxidation, the proposed copper-catalysed mechanism (Scheme 4) presumes the interaction of the substrate with the Cu(II) centre before the subsequent electron transfer to the catalyst. The adiabatic electron affinity of the model complex $[Cu^{II}(HL)(OAc)(CH_3OH)_2]^{1+}$ (**B**) was found to be of the same magnitude (98.9 kcal mol^{-1}; 4.3 eV) as the electron affinities of the aminophenoxyl radicals (Table S10), indicating the possibility of the **B** + RO$^-$ → **B**$^-$ + RO· reaction. The negative overall change of the Gibbs free energy, −11.2 kcal mol^{-1}, calculated for this reaction favours the direct process where copper changes its oxidation state from Cu(II) to Cu(I). However, despite all attempts to find the reasonable reaction pathway and transition state, the aminophenoxyl radical often demonstrates the tendency to coordinate back the copper centre. One can suppose that in the real-life catalytic process the presence of solvation molecules favours separation and stabilization of the reaction products.

The multinuclear copper catalytic species could stabilize the reduced Cu^{II} to Cu^{I} states, in this way leading to higher catalytic activity. The DFT optimized molecular structure of the complex **1** involving four methanol molecules (**1**·4CH_3OH; model complex **C**) approaching the unsaturated apical positions of the copper centres is shown in Figure S27. As can be seen, the copper atoms coordinate only two methanol molecules resulting in square-pyramidal coordination environments around copper centres, while two other methanol molecules remain H-bonded. The TDDFT calculated spectra of the complex **1**·4CH_3OH reveal 6 absorptions from 607.11 to 667.32 nm (excited states S_3 to S_8, Figure 15) making a broad absorption band with predicted maximum at 621 nm (experimental value is 695 nm, Figure 8). All these excitations involve d-d transitions within the dinuclear copper core. DFT modelling of the substitution of one of the coordinated methanol molecules for 2-aminophenol (**1**·**I**·3CH_3OH; model complex **D**) affords the H-atom transfer to the μ-O bridging atoms of aminoalcoholate

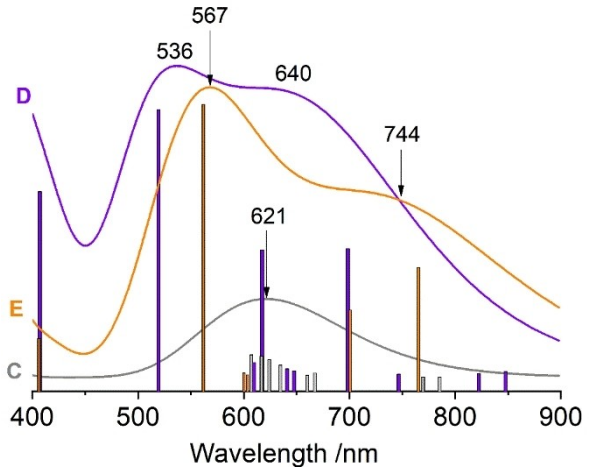

Figure 15. Theoretical UV-Vis absorption spectra of the model compounds **1**·4CH_3OH (**C**), **1**·**I**·3CH_3OH (**D**) and [Cu^{II}(HL)(OAc)(CH_3OH)(**I**)] (**E**) calculated at the TDDFT PBE0/aug-cc-PVDZ (aug-cc-pVTZ for Cu) using TPSS/def2-TZVP optimized geometries. Both TDDFT and geometry optimized involved C-PCM(methanol) solvation model. 200 and 100 excited states were calculated for binuclear (**C** and **D**) and mononuclear (**E**) compounds, respectively. The bars show the exact wavelengths and relative oscillator strengths of the excited states. The solid lines show the Gaussian broadening, for which the numbers indicate the predicted absorption maxima.

ligand, where the latter results in the monodentate coordination mode (Figure S27). The optimized Cu–O distance of the coordinated 2-aminophenolate ligand is 2.025 Å.

The TDDFT calculations of **D** predict the structure of excited states significantly different from that for **1**·4CH_3OH. The spectrum is constructed from several strong low-energy excitations, from which the strongest one is $S_0 \rightarrow S_{10}$ at 519.28 nm (Figure 15). The natural transition orbitals (NTOs) calculated for the 181β → 182β transition (96.9%) of the state S_{10} are shown in Figure S27. This transition is of ligand-to-metal (LMCT) π-d nature with participation of the d_{x2-y2} orbitals of both copper atoms. The simpler mononuclear model [Cu^{II}(HL)(OAc)(CH_3OH)(**I**)] (**E**) was constructed through replacement of the coordinated methanol molecule by 2-aminophenolate anion in the mononuclear model **B**. The TDDFT calculations resulted in the LMCT band at 561.85 nm (Figures 15 and S28). Therefore, the shift of the absorbance to higher energies observed for equimolar mixtures of **1** and **I** (Figure 8) can be associated with the coordination of aminophenol molecule to the metal centre with a proton transfer from the hydroxyl group to the closely located hydroxo-groups of aminoalcohol ligands.

Conclusions

In summary, we report the synthesis of three polynuclear coordination compounds of copper based on the 2-benzylaminoethanol (Hbae) pro-ligand, [Cu^{II}_2(bae)$_2$($Cl)_2$] (**1**), [Cu^{II}_2(Hbae)$_2$(bae)$_2$]($NO_3)_2$ (**2**) and [Cu^{II}_3(Hbae)$_2$(bae)$_2$(dmba)$_2$]($NO_3)_2$ (**3**), two of which (**1** and **3**) possess novel structures and compositions (where Hdmba = 2,2-dimethylbutyric acid). The synthetic investigation disclosed that the compounds **2** and **3** can be obtained from the same reaction system depending on the reaction conditions. The solid-state structures of **1**–**3** have been investigated by the single-crystal X-ray diffraction. The complex **3** is the first example of a transition metal coordination compound bearing 2-benzylethanolaminate and 2,2-dimethylbutyrate ligands simultaneously.

All complexes catalyse aerobic oxidation of 2-aminophenols towards the formation of a phenoxazinone chromophore, mimicking a phenoxazinone synthase-like enzyme activity. The kinetic dependencies suggest no aggregation of molecular structures in solution. The catalytic activity of the complex **1** was studied on a broader scope of substrates, from which 2-amino-5-methylphenol and 2-amino-5-chrolophenol revealed the highest reaction rates, while the nitro-substituted substrates demonstrated almost negligible reactivity.

The combined experimental and DFT theoretical studies were performed with focus on two principal processes: (*a*) abstraction of H atom from aminophenol hydroxyl group upon reaction with copper superoxide Cu^{II}–OO· intermediates and (*b*) activation of aminophenol substrate through its deprotonative coordination to the polynuclear copper core. The reaction energy diagrams for the process (*a*) were found to follow, in general, the observed reactivity of 2-aminophenol substrates. The preliminary modelling of the process (*b*) successfully explains the experimentally observed shifts of the absorption bands in the UV-Vis spectra. The theoretically proposed participation of superoxide Cu^{II}–OO· radicals contradicts the commonly postulated mechanisms of metal-catalysed phenoxazinone synthase-like activity where the O_2 molecule oxidizes the aminophenol substrate coordinated to the metal complex catalyst.

Experimental

General: All chemicals were of reagent grade and used as received. All experiments were carried out in air. Elemental analyses for C, H and N were carried out by the Microanalytical Service of the Instituto Superior Técnico. Infrared spectra were recorded using Agilent Cary 630 ATFT-IR spectrometer in an attenuated total reflectance (ATR) mode and processed through the Bruker OPUS software. UV-Vis spectra were recorded using a Perkin-Elmer Lambda 35 spectrometer.

Synthesis of [Cu_2(bae)$_2$($Cl)_2$] (**1**): $CuCl_2$·$2H_2O$ (0.34 g, 2 mmol), 2-benzylaminoethanol (0.85 mL, 6 mmol) and triethylamine (0.14 mL, 1 mmol) were dissolved in CH_3OH (30 mL) forming a blue-green solution which was magnetically stirred at 50 °C (40 min) for 1 h. The resulting solution was filtered, and green-blue microcrystals of **1** suitable for X-ray crystallographic study were formed within one day. Yield: 0.30 g, 60.2% (based on copper chloride). Anal. calc. for $C_{18}H_{24}Cl_2Cu_2N_2O_2$ (M = 498.37): C, 43.38; N, 5.62; H, 4.85%. Found: C, 43.6; N, 5.7; H, 4.5%.

Syntheses of [Cu_2(Hbae)$_2$(bae)$_2$]($NO_3)_2$ (**2**) and [Cu_3(Hbae)$_2$(bae)$_2$(dmba)$_2$]($NO_3)_2$ (**3**): Cu($NO_3)_2$ ·$3H_2O$ (0.48 g, 2 mmol), 2-benzylaminoethanol (0.85 mL, 6 mmol) and triethylamine (0.14 mL, 1 mmol) were dissolved in CH_3OH (30 mL) forming a blue-green solution which was magnetically stirred at 60 °C (for **2**) or 30 °C (for **3**) for 30 min. Then, 2,2-dimethylbutyric acid (0.25 mL, 2 mmol) was added to this solution and the mixture was stirred for

1 h at the stated temperature. The resulting solution was filtered, and green-blue microcrystals of **2** or dark-blue microcrystals of **3** suitable for X-ray crystallography were isolated within two weeks for both compounds. For **2**: Yield: 0.11 g, 13% (based on copper nitrate). Anal. calc. for $C_{36}H_{50}Cu_2N_6O_{10}$ (M = 853.90): C, 50.64; N, 9.84; H, 5.9%. Found: C, 50.5; N, 9.7; H, 5.8%. For **3**: Yield: 0.49 g, 64% (based on copper nitrate). Anal. calc. for $C_{48}H_{72}Cu_3N_6O_{14}$ (M = 1147.73): C, 50.23; N, 7.32; H, 6.32%. Found: C, 50.0; N, 7.2; H, 6.3%.

Crystallography

Details of the data collection and processing, structure solution and refinement are summarised in Table S1. The single-crystal X-ray data were acquired on a Bruker D8 Quest diffractometer. Cell parameters were retrieved and refined using the Bruker SAINT programme. SADABS was used for correction of absorption.[39] All structures were solved by direct methods by means of SHELXT-2014/5 and refined against F^2 using the SHELXL-2019/2 programme (Table S1).[40] The Olex2 1.5 package was used during the structures' refinement.[41] The hydrogen atoms of O–H and N–H groups were localised and refined freely except of the atoms of disordered aminoalcohol ligand in **3**. The remaining H atoms were placed at calculated positions and refined using the riding model with $U_{iso} = 1.5U_{eq}$ (for methyl groups) or $U_{iso} = 1.2U_{eq}$ (for other groups). The benzylic group of one of the aminoalcohol ligand in **2** was found to be disordered over two positions with occupations 0.47(2) and 0.53(2). The molecular structure of **3** exhibits higher degree of positional disorder with one aminoalcohol ligand disordered over two conformations with occupations of 0.391(19) and 0.609(19), and one tert-butyl group disordered over two positions with occupations of 0.455(13) and 0.545(13).

Deposition Numbers 2373524 (for **1**), 2373526 (for **2**), and 2373525 (for **3**) contain the supplementary crystallographic data for this paper. These data are provided free of charge by the joint Cambridge Crystallographic Data Centre and Fachinformationszentrum Karlsruhe Access Structures service www.ccdc.cam.ac.uk/structures.

Catalytic reactions

The phenoxazinone synthase activity of **1**–**3** was monitored spectroscopically by recording the UV-Vis spectra at certain periods of time. Typically, 5 mL of the methanol solution of the complex of desired concentration was added to a 10 mL flask containing 5.5 mg of *2*-aminophenol (OAP). After 5 sec of vigorous stirring a portion of the resulting mixture was transferred into a quartz cuvette (10 mm; Labbox MISQ-010–002) of the spectrophotometer, without further stirring.

Theoretical Calculations

The ORCA 5.0.3 and 5.0.4 packages[42] were used for all calculations. Unless stated otherwise, the TPSS functional[43] with the def2-TZVP basis set[44] was used for all atoms for geometry optimizations and transition state search, and ωB97M–V functional[45] with de2-QZVPPD basis set[46] for single point energies. In the latter case the SCF convergence criteria were set by *VeryTightSCF* keyword. Integration grid of high density (*Defgrid3* keyword) was employed along with geometry optimization and TDDFT calculations. Transition states were found using through the nudged elastic band (NEB) method.[47] The solvent (methanol) effects were accounted by means of the conductor-like polarizable continuum model (C-PCM).[48] The correction ΔG term of 1.89 kcal mol^{-1} was added to the final Gibbs energies of single molecules to convert 1 atm to 1 M standard states.[49] The CASSCF/NEVPT2 studies[50] were performed using the def2-TZVP basis set for all atoms. The vertical excitation energies were calculated by the TDDFT (PBE0 functional[51] with aug-cc-pVTZ basis set for copper[52] and aug-cc-pVDZ for other elements[53]; TDA approximation was applied[54]) and STEOM-DLPNO-CCSD[37,55] methodologies (cc-pVTZ basis set[56]). *AutoAux* keyword[57] was used to generate the auxiliary basis sets in all calculations except those using the cc-pVTZ set, for which the cc-pVTZ/C Coulomb fitting basis set[58] was applied. Dispersion correction was introduced through the D4 model.[59] All calculations involved RIJ-COSX[60] or RI[61] speed-up approximations. Visualization of the molecular orbitals was performed by means of Avogadro 1.2 program.[62] Unless stated otherwise, the isosurfaces of the molecular orbitals are shown at the 0.03 a.u. level and isosurfaces of spin densities at 0.005 a.u. level. Analysis of bond critical points and non-covalent interactions indexes[63] was done using the Multiwfn 3.8 program.[64] The force-field conformational search was performed through the GFN-FF model[65] implemented in the CREST 3.0.1. program[66] involving the xTB suite.[67] The calculations of the EI-MS spectra were performed at the semi-empirical GFN2-xTB level[68] using the QCxMS 5.2.1 package.[69] The starting temperature T_{init} was set to 300 K and the impact excess energy per atom (parameter *ieeatm*) was set to 0.8. All other parameters were kept at their default values.

Supporting Information Summary

Supporting Information is available from the Wiley Online Library. Selected bond lengths and angles for crystal structures **1**–**3**, IR spectra and packing diagrams for **1**–**3**, experimental and theoretical UV-Vis of substrates, products and intermediates, tabulated Gibbs and single point energies of reaction components, sample ORCA input files and selected outputs, the Cartesian xyz-files of the optimized structures of 2-aminophenol substrates (in neutral, radical and anionic forms), phenoxazinone chromophores, model copper complexes, intermediates and transition states.

Acknowledgements

This work was supported by the Fundação para a Ciência e a Tecnologia, I.P/; MCTES through national funds PIDDAC – CQE UIDB/00100/2020 and UIDP/00100/2020 (DOI 10.54499/UIDP/00100/2020) and IMS the Associated Laboratory funded by Project LA/P/0056/2020 (DOI 10.54499/LA/P/0056/2020). The simulations reported in this paper were in part performed at the OBLIVION Supercomputer (HPC Centre of the University of Évora, Portugal) of the "Enabling Green E-science for the SKA Research Infrastructure (ENGAGE SKA)", reference POCI-01–0145-FEDER-022217, funded by COMPETE 2020 and Foundation for Science and Technology (FCT), Portugal. This research was funded by the FCT under project 2023.10683.CPCA.A1.

Conflict of Interests

The authors declare no conflict of interest.

Data Availability Statement

The data that support the findings of this study are available in the supplementary material of this article.

Keywords: Copper · Aminophenol · Phenoxazinone synthase-like catalysis · DFT theoretical calculations of reaction mechanism · Copper superoxol compounds

[1] a) M. Le Roes-Hill, C. Goodwin, S. Burton, *Trends Biotechnol.* **2009**, *27*, 248–258; b) U. Hollstein, *Chem. Rev.* **1974**, *74*, 625–652; c) C. E. Barry, P. G. Nayar, T. P. Begley, *Biochem.* **1989**, *28*, 6323–6333.
[2] E. Katz, H. Weissbach, *J. Biol. Chem.* **1962**, *237*, 882–886.
[3] A. W. Smith, A. Camara-Artigas, M. T. Wang, J. P. Allen, W. A. Francisco, *Biochem.* **2006**, *45*, 4378–4387.
[4] a) S. K. Dey, A. Mukherjee, *Coord. Chem. Rev.* **2016**, *310*, 80–115; b) P. Koley, B. Ghosh, J. Bhattacharyya, A. Hazari, *Mol. Catal.* **2024**, *569*.
[5] a) I. Roy, A. Muley, S. Mathur, A. Verma, M. K. Kumawat, S. Maji, *New J. Chem.* **2024**, *48*, 11647–11661; b) N. C. Jana, Y. C. Sun, R. Herchel, R. Nandy, P. Brandao, B. Bagh, X. Y. Wang, A. Panja, *Dalton Trans.* **2024**, *53*, 11514–11530; c) A. Muley, K. S. Karumban, S. Kumbhakar, S. Mathur, I. Roy, A. Verma, M. K. Kumawat, S. Maji, *New J. Chem.* **2024**, *48*, 7739–7753; d) T. P. Mohammed, A. George, M. P. Sivaramakrishnan, P. Vadivelu, S. Balasubramanian, M. Sankaralingam, *J. Inorg. Biochem.* **2023**, *247*, 112309; e) S. Nakul, M. G. Krishnendu, D. Senthurpandi, J. Mathew, N. Kulkarni, *Inorg. Chim. Acta* **2025**, *578*, 122550.
[6] a) I. R. Chowdhury, A. Chatterjee, A. Mahanta, S. Jasimuddin, R. Ghosh, *Inorg. Chim. Acta* **2024**, *566*, 122006; b) A. Chatterjee, S. Khan, R. Ghosh, *Polyhedron* **2019**, *173*, 114151.
[7] A. Patra, A. Das, A. Sarkar, C. J. Gómez-García, C. Sinha, *Dalton Trans.* **2024**, *53*, 13515–13528.
[8] a) N. C. Jana, P. Brandao, R. M. Gomila, A. Frontera, A. Panja, *New J. Chem.* **2024**, *48*, 2389–2402; b) A. Muley, K. S. Karumban, S. Kumbhakar, B. Giri, S. Maji, *New J. Chem.* **2022**, *46*, 521–532.
[9] a) S. Kumbhakar, B. Giri, A. Muley, K. S. Karumban, S. Maji, *Dalton Trans.* **2021**, *50*, 16601–16612; b) N. C. Jana, P. Brandao, A. Frontera, A. Panja, *Dalton Trans.* **2020**, *49*, 14216–14230; c) N. C. Jana, Z. Jaglicic, P. Brandao, A. Panja, *ACS Omega* **2024**, *9*, 49953–49965.
[10] a) S. Dutta, T. K. Ghosh, P. Mahapatra, A. Ghosh, *Inorg. Chem.* **2020**, *59*, 14989–15003; b) S. Dutta, P. Bhunia, J. Mayans, M. G. B. Drew, A. Ghosh, *Dalton Trans.* **2020**, *49*, 11268–11281; c) S. Dutta, J. Mayans, A. Ghosh, *Dalton Trans.* **2020**, *49*, 1276–1291; d) T. Chakraborty, A. Sarkar, A. Adhikary, N. Chakiroy, D. Das, *Cryst. Grow. Des.* **2019**, *19*, 7336–7348.
[11] a) D. S. Nesterov, O. V. Nesterova, A. J. L. Pombeiro, *Coord. Chem. Rev.* **2018**, *355*, 199–222; b) P. Buchwalter, J. Rose, P. Braunstein, *Chem. Rev.* **2015**, *115*, 28–126.
[12] a) W. X. Duan, W. H. Li, Q. X. Tang, Y. Y. Zhao, X. J. Guo, G. Y. Yang, *Chemistryselect* **2021**, *6*, 2504–2507; b) F. Bruyneel, G. Dive, J. Marchand-Brynaert, *Org. Biomol. Chem.* **2012**, *10*, 1834–1846; c) J. M. Granda, K. Piekielska, M. Wasinska, N. Kawecka, M. Giurg, *Synthesis* **2015**, *47*, 3321–3332.
[13] O. V. Nesterova, A. J. L. Pombeiro, D. S. Nesterov, *Catalysts* **2022**, *12*, 1408.
[14] a) Y. Y. Jiang, C. Chen, *Org. Biomol. Chem.* **2023**, *21*, 7852–7872; b) H. Y. Kim, K. Oh, *Org. Biomol. Chem.* **2021**, *19*, 3569–3583; c) S. D. McCann, S. S. Stahl, *Acc. Chem. Res.* **2015**, *48*, 1756–1766; d) S. E. Allen, R. R. Walvoord, R. Padilla-Salinas, M. C. Kozlowski, *Chem. Rev.* **2013**, *113*, 6234–6458.
[15] M. Kumar, A. K. Singh, A. K. Singh, R. K. Yadav, S. Singh, A. P. Singh, A. Chauhan, *Coord. Chem. Rev.* **2023**, *488*, 215176.
[16] O. V. Nesterova, O. E. Bondarenko, A. J. L. Pombeiro, D. S. Nesterov, *Dalton Trans.* **2020**, *49*, 4710–4724.
[17] a) O. V. Nesterova, M. L. Kuznetsov, A. J. L. Pombeiro, G. B. Shul'pin, D. S. Nesterov, *Catal. Sci. Technol.* **2022**, *12*, 282–299; b) D. S. Nesterov, O. V. Nesterova, *Catalysts* **2021**, *11*, 1148; c) O. V. Nesterova, K. V. Kasyanova, V. G. Makhankova, V. N. Kokozay, O. Y. Vassilyeva, B. W. Skelton, D. S. Nesterov, A. J. L. Pombeiro, *Appl. Catal. A* **2018**, *560*, 171–184; d) D. S. Nesterov, J. Jezierska, O. V. Nesterova, A. J. L. Pombeiro, A. Ozarowski, *Chem. Commun.* **2014**, *50*, 3431–3434; e) V. V. Semenaka, O. V. Nesterova, V. N. Kokozay, R. I. Zybatyuk, O. V. Shishkin, R. Boca, C. J. Gomez-Garcia, J. M. Clemente-Juan, J. Jezierska, *Polyhedron* **2010**, *29*, 1326–1336; f) O. V. Nesterova, A. V. Lipetskaya, S. R. Petrusenko, V. N. Kokozay, B. W. Skelton, J. Jezierska, *Polyhedron* **2005**, *24*, 1425–1434; g) D. S. Nesterov, V. N. Kokozay, B. W. Skelton, *Eur. J. Inorg. Chem.* **2009**, 5469–5473.
[18] T. A. Fernandes, V. Andre, A. M. Kirillov, M. V. Kirillova, *J. Mol. Catal. A* **2017**, *426*, 357–367.
[19] S. Grimme, A. Hansen, S. Ehlert, J. M. Mewes, *J. Chem.l Phys.* **2021**, *154*, 064103.
[20] S. Emamian, T. Lu, H. Kruse, H. Emamian, *J. Comput. Chem.* **2019**, *40*, 2868–2881.
[21] C. R. Groom, I. J. Bruno, M. P. Lightfoot, S. C. Ward, *Acta Crystallogr. Sect. B* **2016**, *72*, 171–179.
[22] K. Anzai, K. Isono, K. Okuma, S. Suzuki, *J. Antibiot.* **1960**, *13*, 125–132.
[23] S. Q. Guo, H. B. Hu, W. Wang, M. Bilal, X. H. Zhang, *J. Agricult. Food Chem.* **2022**, *70*, 7742–7750.
[24] M. Giurg, K. Piekielska, M. Gebala, B. Ditkowski, M. Wolanski, W. Peczynska-Czoch, J. Mlochowski, *Synth. Commun.* **2007**, *37*, 1779–1789.
[25] C. Mukherjee, T. Weyhermuller, E. Bothe, E. Rentschier, P. Chaudhuri, *Inorg. Chem.* **2007**, *46*, 9895–9905.
[26] Z. Szeverenyi, E. R. Milaeva, L. I. Simandi, *J. Mol. Catal.* **1991**, *67*, 251–258.
[27] J. M. Lehn, *Chem. Eur. J.* **1999**, *5*, 2455–2463.
[28] a) S. Low, J. Becker, C. Wurtele, A. Miska, C. Kleeberg, U. Behrens, O. Walter, S. Schindler, *Chem. Eur. J.* **2013**, *19*, 5342–5351; b) S. Becker, M. Durr, A. Miska, J. Becker, C. Gawlig, U. Behrens, I. Ivanovic-Burmazovic, S. Schindler, *Inorg. Chem.* **2016**, *55*, 3759–3766.
[29] J. Kaizer, R. Csonka, G. Speier, *J. Mol. Catal. A* **2002**, *180*, 91–96.
[30] F. Ferlin, A. Marini, N. Ascani, L. Ackermann, D. Lanari, L. Vaccaro, *ChemCatChem* **2020**, *12*, 449–454.
[31] P. Mahapatra, S. Ghosh, S. Giri, V. Rane, R. Kadam, M. G. B. Drew, A. Ghosh, *Inorg. Chem.* **2017**, *56*, 5105–5121.
[32] a) C. Y. Hao, R. E. March, *J. Mass Spectrom.* **2001**, *36*, 509–521; b) L. Gianelli, V. Amendola, L. Fabbrizzi, P. Pallavicini, G. G. Mellerio, *Rapid Commun. Mass Spectrom.* **2001**, *15*, 2347–2353.
[33] D. Dvoranová, Z. Barbieriková, V. Brezová, *Molecules* **2014**, *19*, 17279–17304.
[34] a) T. Horath, J. Kaizer, G. Speier, *J. Mol. Catal. A* **2004**, *215*, 9–15; b) M. R. Maurya, S. Sikarwar, T. Joseph, S. B. Halligudi, *J. Mol. Catal. A* **2005**, *236*, 132–138; c) L. I. Simandi, T. Barna, S. Nemeth, *J. Chem. Soc. Dalton Trans.* **1996**, 473–478.
[35] a) P. Wu, J. Y. Zhang, Q. Q. Chen, W. Peng, B. J. Wang, *Chin. J. Catal.* **2022**, *43*, 913–927; b) S. Fukuzumi, Y. M. Lee, W. Nam, *Dalton Trans.* **2019**, *48*, 9469–9489.
[36] a) M. Bhadra, W. J. Transue, H. Lim, R. E. Cowley, J. Y. C. Lee, M. A. Siegler, P. Josephs, G. Henkel, M. Lerch, S. Schindler, A. Neuba, K. O. Hodgson, B. Hedman, E. I. Solomon, K. D. Karlin, *J. Am. Chem. Soc.* **2021**, *143*, 3707–3713; b) R. L. Peterson, R. A. Himes, H. Kotani, T. Suenobu, L. Tian, M. A. Siegler, E. I. Solomon, S. Fukuzumi, K. D. Karlin, *J. Am. Chem. Soc.* **2011**, *133*, 1702–1705; c) J. M. Hoover, B. L. Ryland, S. S. Stahl, *J. Am. Chem. Soc.* **2013**, *135*, 2357–2367; d) M. A. Iron, A. M. Szpilman, *Chem. Eur. J.* **2017**, *23*, 1368–1378.
[37] C. Riplinger, B. Sandhoefer, A. Hansen, F. Neese, *J. Chem. Phys.* **2013**, *139*, 134101.
[38] a) S. Grimme, *J. Chem. Phys.* **2003**, *118*, 9095–9102; b) M. Feyereisen, G. Fitzgerald, A. Komornicki, *Chem. Phys. Lett.* **1993**, *208*, 359–363.
[39] BrukerAXS Inc., Madison, WI **2004**APEX2 & SAINT.
[40] G. M. Sheldrick, *Acta Crystallogr. C* **2015**, *71*, 3–8.
[41] O. V. Dolomanov, L. J. Bourhis, R. J. Gildea, J. A. K. Howard, H. Puschmann, *J. Appl. Crystallogr.* **2009**, *42*, 339–341.
[42] a) F. Neese, *Wil. Interdiscipl. Rev. Comput. Mol. Sci.* **2022**, *12*, e1606; b) F. Neese, F. Wennmohs, U. Becker, C. Riplinger, *J. Chem. Phys.* **2020**, *152*, 18; c) F. Neese, *J. Comput. Chem.* **2023**, *44*, 381–396.
[43] J. M. Tao, J. P. Perdew, V. N. Staroverov, G. E. Scuseria, *Phys. Rev. Lett.* **2003**, *91*, 146401.
[44] F. Weigend, R. Ahlrichs, *Phys. Chem. Chem. Phys.* **2005**, *7*, 3297–3305.
[45] N. Mardirossian, M. Head-Gordon, *J. Chem. Phys.* **2016**, *144*, 214110.
[46] D. Rappoport, F. Furche, *J. Chem. Phys.* **2010**, *133*, 134105.
[47] V. Asgeirsson, B. O. Birgisson, R. Bjornsson, U. Becker, F. Neese, C. Riplinger, H. Jonsson, *J. Chem. Theor. Comput.* **2021**, *17*, 4929–4945.
[48] a) V. Barone, M. Cossi, *J. Phys. Chem. A* **1998**, *102*, 1995–2001; b) M. Garcia-Ratés, F. Neese, *J. Comput. Chem.* **2020**, *41*, 922–939.
[49] A. V. Marenich, C. J. Cramer, D. G. Truhlar, *J. Phys. Chem. B* **2009**, *113*, 6378–6396.

[50] a) C. Angeli, R. Cimiraglia, S. Evangelisti, T. Leininger, J. P. Malrieu, *J. Chem. Phys.* **2001**, *114*, 10252–10264; b) Y. Guo, K. Sivalingam, F. Neese, *J. Chem. Phys.* **2021**, *154*, 214111.
[51] C. Adamo, V. Barone, *J. Chem. Phys.* **1999**, *110*, 6158–6170.
[52] a) N. B. Balabanov, K. A. Peterson, *J. Chem. Phys.* **2005**, *123*, 064107; b) N. B. Balabanov, K. A. Peterson, *J. Chem. Phys.* **2006**, *125*, 074110.
[53] R. A. Kendall, T. H. Dunning, R. J. Harrison, *J. Chem. Phys.* **1992**, *96*, 6796–6806.
[54] S. Hirata, M. Head-Gordon, *Chem. Phys. Lett.* **1999**, *314*, 291–299.
[55] a) M. Nooijen, R. J. Bartlett, *J. Chem. Phys.* **1997**, *106*, 6441–6448; b) C. Riplinger, F. Neese, *J. Chem. Phys.* **2013**, *138*, 034106.
[56] T. H. Dunning, *J. Chem. Phys.* **1989**, *90*, 1007–1023.
[57] G. L. Stoychev, A. A. Auer, F. Neese, *J. Chem. Theor. Comput.* **2017**, *13*, 554–562.
[58] F. Weigend, A. Köhn, C. Hättig, *J. Chem. Phys.* **2002**, *116*, 3175–3183.
[59] E. Caldeweyher, S. Ehlert, A. Hansen, H. Neugebauer, S. Spicher, C. Bannwarth, S. Grimme, *J. Chem. Phys.* **2019**, *150*, 154122.
[60] a) B. Helmich-Paris, B. de Souza, F. Neese, R. Izsak, *J. Chem. Phys.* **2021**, *155*, 104109; b) F. Neese, F. Wennmohs, A. Hansen, U. Becker, *Chem. Phys.* **2009**, *356*, 98–109; c) F. Neese, *J. Comput. Chem.* **2003**, *24*, 1740–1747.
[61] F. Neese, G. Olbrich, *Chem. Phys. Lett.* **2002**, *362*, 170–178.
[62] M. D. Hanwell, D. E. Curtis, D. C. Lonie, T. Vandermeersch, E. Zurek, G. R. Hutchison, *J. Cheminform.* **2012**, *4*, 17.
[63] E. R. Johnson, S. Keinan, P. Mori-Sanchez, J. Contreras-Garcia, A. J. Cohen, W. T. Yang, *J. Am. Chem. Soc.* **2010**, *132*, 6498–6506.
[64] T. Lu, F. W. Chen, *J. Comput. Chem.* **2012**, *33*, 580–592.
[65] S. Spicher, S. Grimme, *Angew. Chem. Int. Edit.* **2020**, *59*, 15665–15673.
[66] a) P. Pracht, S. Grimme, C. Bannwarth, F. Bohle, S. Ehlert, G. Feldmann, J. Gorges, M. Müller, T. Neudecker, C. Plett, S. Spicher, P. Steinbach, P. A. Wesolowski, F. Zeller, *J. Chem. Phys.* **2024**, *160*, 114110; b) P. Pracht, F. Bohle, S. Grimme, *Phys. Chem. Chem. Phys.* **2020**, *22*, 7169–7192.
[67] C. Bannwarth, E. Caldeweyher, S. Ehlert, A. Hansen, P. Pracht, J. Seibert, S. Spicher, S. Grimme, *Wil. Interdiscipl. Rev. Comput. Mol. Sci.* **2021**, *11*, e01493.
[68] C. Bannwarth, S. Ehlert, S. Grimme, *J. Chem. Theor. Comput.* **2019**, *15*, 1652–1671.
[69] a) S. Grimme, *Angew. Chem. Int. Edit.* **2013**, *52*, 6306–6312; b) J. Koopman, S. Grimme, *ACS Omega* **2019**, *4*, 15120–15133.

Manuscript received: September 20, 2024
Revised manuscript received: February 8, 2025
Accepted manuscript online: February 10, 2025
Version of record online: February 19, 2025